J. Fluid Mech. (1976), *vol.* 73, *part* 3, *pp.* 465–495
Printed in Great Britain

The planar turbulent jet

By E. GUTMARK
Faculty of Aeronautical Engineering, Technion, Haifa, Israel
AND I. WYGNANSKI
School of Engineering, Tel-Aviv University, Ramat-Aviv, Israel

(Received 20 May 1974 and in revised form 5 May 1975)

Results of hot-wire measurements in a plane incompressible jet are reported. The flow was found to be self-preserving beyond $x/d > 40$ and measurements were made up to $x/d = 120$. The quantities measured include mean velocities, turbulence intensities and third- and fourth-order terms, as well as two-point correlations and the intermittency factor. Conditional sampling techniques were used to obtain exclusively data within the turbulent zone of the jet. The results are compared with previous investigations.

This is the third paper in a sequence providing data on turbulent free shear flows.

1. Introduction

The present investigation was undertaken in order to extend the available information on the two-dimensional self-preserving jet. The plane jet has been investigated extensively and sufficient data are available for many practical engineering purposes. On the other hand, very few definitive experiments have been carried out in which an attempt has been made to study the structure of the flow.

This flow was first investigated by Förthmann (1934), who measured the mean velocities in the developing region, covering a distance of 25 slot widths downstream from the nozzle. Miller & Comings (1957) extended the range of measurements to 40 slot widths and measured the streamwise component of the turbulent fluctuations. However, it is unlikely that self-preservation was attained with this extension. Van der Hegge Zijnen (1958) measured the mean velocities and turbulent intensities over the same distance as Miller & Comings. The intensities presented by the former author are lower; however he used a constant-current anemometer while Miller & Comings used constant-temperature equipment. The poor response of the constant-current anemometer to high frequency fluctuations could possibly be responsible for the low intensities reported by Van der Hegge Zijnen.

Knystautas (1964) mapped the mean flow field up to a distance of 400 slot widths downstream from the nozzle and established clearly the similarity of mean velocity profiles in this flow. Bradbury (1965) studied the structure of a two-dimensional jet exhausting into a weak external stream. In this way,

measurement errors resulting from the high turbulence intensity at the edges of the jet were avoided. The use of a nonlinearized constant-current anemometer probably forced Bradbury to sacrifice precise self-preservation and thus attain low local turbulence levels. The most detailed investigation was made by Heskestad (1965), who used constant-temperature, linearized, hot-wire anemometers and thus provided data in the self-preserving region more than 100 slot widths from the plane of the nozzle.

Preliminary observations by Bradbury (1965) indicated that all free turbulent shear flows may have a similar structure. This similarity should not be restricted by local isotropy considerations but should apply to the larger eddies as well. In order to determine the validity of this hypothesis, the measurements should exclude the fluctuations in the irrotational flow outside the jet boundaries, which may be affected by the geometry of the particular experiment. Conditional sampling techniques can provide data obtained exclusively within the turbulent zone. With this in mind, the present investigation was undertaken. Furthermore, similar investigations had been carried out in an axisymmetric jet and in a mixing layer. This third investigation, of a two-dimensional jet, will complete the compilation of data on incompressible turbulent jets taken with identical instrumentation. These flows can thus be compared without having to account for discrepancies in measuring techniques (i.e. the inaccuracies or errors are presumably the same for all three flows).

Most of the measurements were made 120 slot widths downstream from the nozzle, which proved to be well within the self-preserving region. The exhaust velocity was 35 m/s and the Reynolds number based on the width of the slot was 3×10^4.

2. Apparatus and instrumentation

The apparatus used is shown schematically in figure 1. A variable-speed axial blower provided the airflow through a rectangular orifice 1·3 cm wide and 50 cm long. The orifice was milled in a 1 cm thick brass plate using a high-precision milling machine to an accuracy of 0·001 cm over its entire length. The plate was mounted flush in a plane vertical wall which extended 100 cm on each side of the orifice. The centre-plane of the jet was perpendicular to this wall. The jet was confined by two horizontal walls placed just above and just below the nozzle and extending 200 cm downstream of the slot. The mean flow was two-dimensional except in the vicinity of the walls, where a 'saddle-back' profile developed (see also Heskestad 1965), but the variation in total head across the span of the jet did not exceed 2 % over 35 cm at $x/d \leqslant 100$.

The entrained air passed through two 16 mesh screens set 2 cm apart and stretched around the supports of the confining walls as shown in figure 1. The screens eliminated most room draughts, which were otherwise noticeable at large distances from the nozzle. The temperature in the room was maintained constant to within ± 1 °C and the air passing through the fan was filtered. The exit Reynolds number was 3×10^4 and the turbulence level was about 0·2 %.

Measurements were made with DISA 55-D01 constant-temperature anemo-

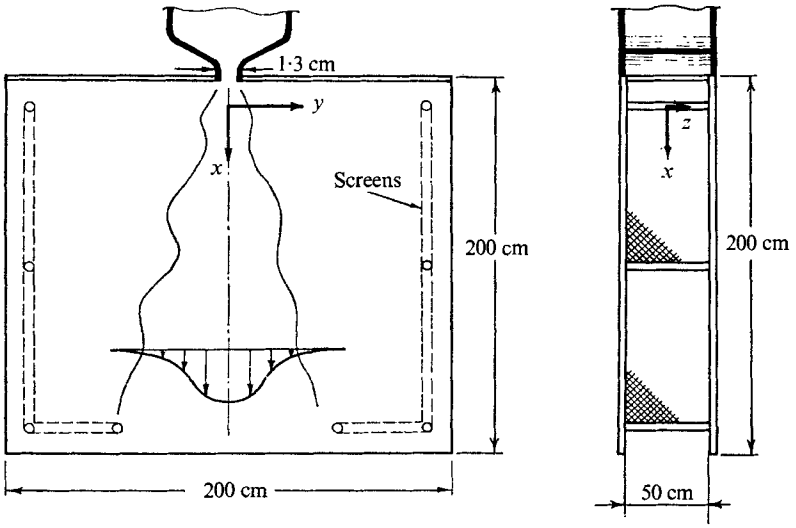

FIGURE 1. Schematic diagram of experimental apparatus.

meters in conjunction with DISA 55-D10 linearizers. The linearizers were calibrated in known flow conditions in the core of the jet. Fluctuations in lateral components were measured with symmetric X-arrays and with single inclined wires. The sensitivity of these sensors to the lateral components of the velocity fluctuations was obtained by yawing them in a plane parallel to the plane of the cross. The wires were manufactured by DISA and constructed from 5 μm or sometimes 2·5 μm tungsten wire. Some wires were gold plated, with the active (unplated) portion varying in length from 0·4 to 1·2 mm.

The signal was processed using various analog electronic circuits for adding, subtracting, multiplying, differentiating and integrating purposes. All components except the differentiator were calibrated for frequencies ranging from d.c. to 15 kHz. The lower bound on the differentiator was approximately 50 Hz. The method of acquisition of zone-averaged data was discussed in an earlier paper (Wygnanski & Fiedler 1970). The intermittency signal was continuously monitored and compared with the longitudinal component u' of the velocity fluctuations, which was high-pass filtered at 100 Hz and squared before being displayed on a dual-trace Tektronix memory scope. The signal chosen for measuring intermittency was $u'^2+(\partial u'/\partial t)^2$, which was slightly smoothed to prevent excessive drop-outs.

3. Intermittency

Cumulative data on the lateral variation of the intermittency factor far downstream of the nozzle are shown in figure 2. The results are well represented by an error function as shown in the probability plot (figure 3). The average location of the interface (i.e. the location at which the intermittency factor $\gamma = 0{\cdot}5$) is $\eta \equiv y/(x-x_0) = 0{\cdot}178$, where x_0 is the distance between the hypothetical

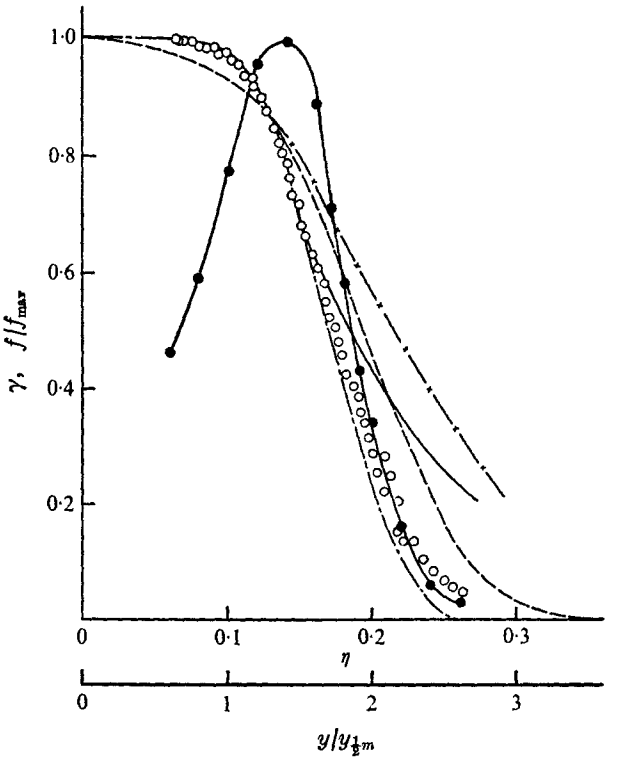

FIGURE 2. Cumulative distributions of the intermittency factor and interface crossing rate. ●, f/f_{max}; ○, γ; ——, γ from flatness factor; —×—, γ without screens; – – –, γ from Heskestad (1965); — – —, Bradbury (1965).

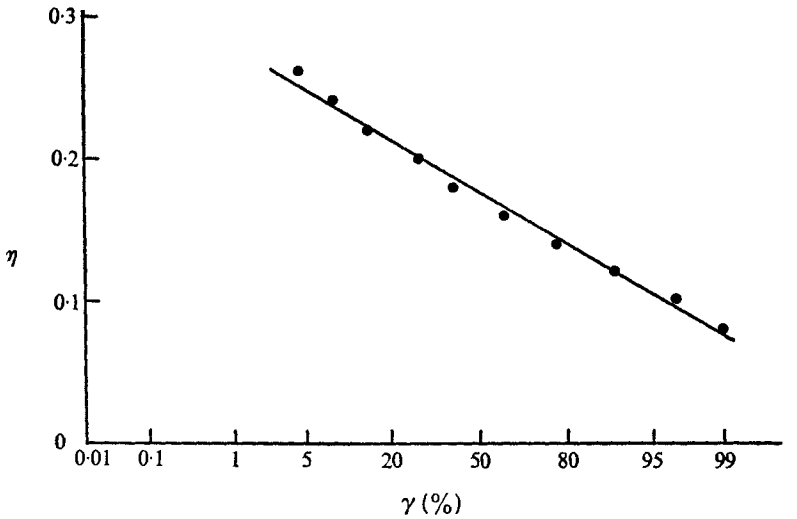

FIGURE 3. A probability plot of the intermittency distribution. $\sigma = 0{\cdot}043x$, $\bar{\eta} = 0{\cdot}178$.

origin of the flow and the nozzle. The excursions of the interface about this position are represented by a standard deviation $\sigma = 0{\cdot}043x$.

The need for the screens (shown in figure 1) became apparent during the preliminary measurements of intermittency, when fluctuations of relatively large amplitude were observed at the outer edges of the jet. The addition of the screens eliminated these fluctuations and narrowed the intermittent zone without affecting the mean velocity profile. The intermittency distribution in the absence of the screens is shown in figure 2. Evidently the screens have a profound effect on γ even in the central region of the jet ($\eta \leqslant 0{\cdot}13$), where the γ measured in their absence agreed quite well with the results of Heskestad (1965). Nevertheless for $\eta \geqslant 0{\cdot}14$, the intermittency measured by Heskestad drops faster than the present investigation would indicate in the absence of screens. It is quite plausible to attribute the discrepancy to room draughts, which might have been stronger in the vicinity of the present apparatus. The scale of the room draughts, which corresponds to the distance between the horizontal plates (i.e. a characteristic length of the apparatus) and is approximately equal to the width of the jet at $x/d \simeq 120$, might have a stronger effect on denting of the interface in spite of the fact that their intensity is small relative to the turbulent intensity of the jet. The intermittency distribution obtained by assuming that

$$\gamma = \left(\frac{\overline{u'^4}}{(\overline{u'^2})^2}\right)_{\mathbb{Q}} \Big/ \left(\frac{\overline{u'^4}}{(\overline{u'^2})^2}\right)$$

agrees with the measured intermittency distribution for $\eta \leqslant 0{\cdot}16$. For $\eta > 0{\cdot}16$ the distribution of intermittency calculated from the flatness factor appears to be wider than that actually measured.

A plane jet exhausting into a slow-moving parallel stream (Bradbury 1965) is narrower than a comparable one exhausting into quiescent surroundings. The direction of the entrained flow, which is parallel to the axis of the jet in this case, has a calming effect on the interface and severely limits the entrainment capacity of the jet and hence its growth with downstream distance. For the purpose of comparison between Bradbury's results and ours the abscissa variable in figure 2 was changed to $y/y_{\frac{1}{2}m}$, where $y_{\frac{1}{2}m}$ is the distance from the plane of symmetry at which the velocity relative to the free stream is half its maximum value. The agreement between the two results when compared on this basis is very good.

The normalized frequency $f/f_{\max}$ with which the interface crosses a given point is also shown in figure 2. The normalization was necessary because f is very sensitive to the amount by which the signal chosen for the detection is smoothed. The ratio $f/f_{\max}$ was found to be insensitive to the smoothing. The curve has a peak at $\eta = 0{\cdot}14$, corresponding to $\gamma = 0{\cdot}7$. This result contradicts previous observations in mixing layers and boundary layers, where the maximum crossing rate of the interface occurred at $\gamma = 0{\cdot}5$. This implies that the turbulent interface is more convoluted in its 'valleys' than in its 'ridges' and that the small-scale turbulence, which is stronger at the centre of the jet, has some effect on the interface.

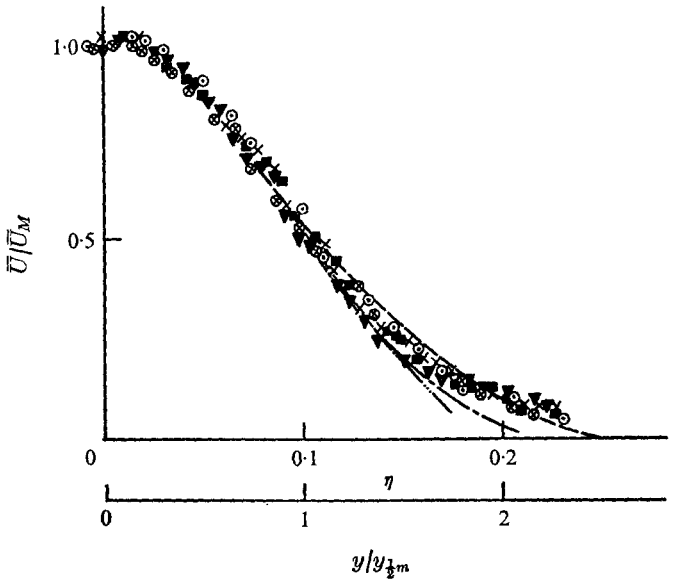

FIGURE 4. The conventional mean velocity profile. ▼, $x/d = 118$; ×, $x/d = 103$; ■, $x/d = 88$; ⊗, $x/d = 76$; ⊙, $x/d = 65$. —·····—, Knystautas (1964); — —, Heskestad (1965); — — —, Bradbury (1965).

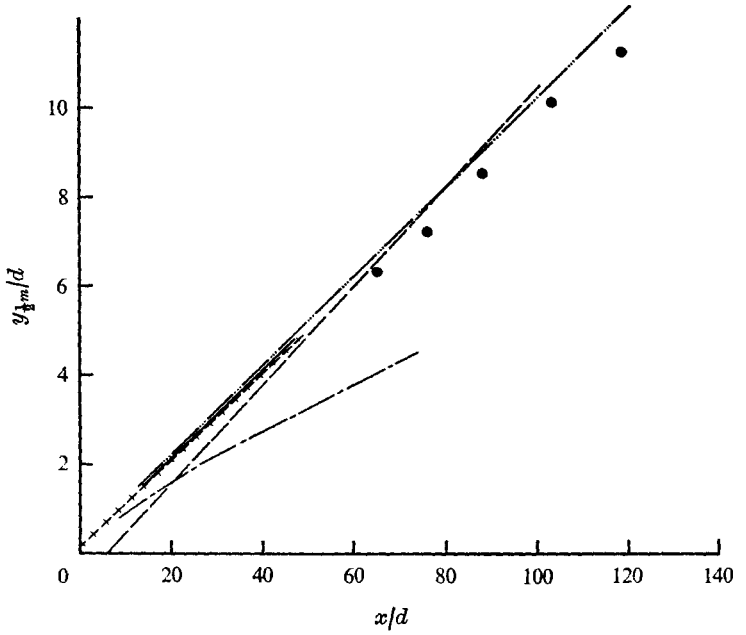

FIGURE 5. The growth of the jet with downstream distance. —·····—, Knystautas (1964); — — —, Bradbury (1965); — —, Heskestad (1965); + + + + +, Miller & Comings (1957); ———, Van der Hegge Zijnen (1958); ●, present results.

4. The mean velocity

The mean velocity profile was measured with a Pitot tube and with a hot wire. Both instruments recorded identical velocities. However the scatter in the hot-wire data was significantly reduced by using long integration times. Measurements were made across the entire jet in some cases in order to establish the symmetry of the flow about its centre-plane. The hot-wire results were corrected for high turbulence intensity.

Velocity profiles normalized with respect to the maximum velocity at a given value of x/d are plotted in figure 4. The abscissa variable is the dimensionless distance η from the plane of symmetry. The profiles are similar and have the usual bell shape. The results of Heskestad, Bradbury and Kynstautas are plotted for comparison. The agreement between the four sets of data is good for $\eta \leqslant 0{\cdot}1$, but for $\eta > 0{\cdot}1$ the profile measured by Heskestad is somewhat wider than the rest.

The growth of the jet with downstream distance is given in figure 5 and compared with five other sets of results. The jet spreads linearly with x and the locus of the half-velocity points is given by

$$y_{\frac{1}{2}m} \simeq 0{\cdot}1(x - x_0).$$

The results of Van der Hegge Zijnen (1958), Miller & Comings (1957), Knystautas (1964) and the present investigation are in good agreement, yielding $x_0 \simeq -2d$, but the spread of the jet reported by Heskestad (1965) is given by $y_{\frac{1}{2}m} = 0{\cdot}11(x - 6d)$. However, the experimental apparatus of Heskestad differed from all the others since it had a long approach channel separating the nozzle from the plenum chamber. The jet, upon leaving the nozzle, probably had a velocity profile typical of channel flows having a high turbulence level averaging 2–4 %. In all other investigations attempts were made to lower the turbulence level at the exit and produce a 'top-hat' profile. The different initial conditions are most probably responsible for the shift in the hypothetical origin and the slightly different rate of spread of the jet. Crow & Champagne (1971) were able to change the initial rate of spread of a jet and the location of its hypothetical origin by imposing on it a sinusoidal surging equivalent to 2 % of the mean exit speed. Different spreading rates of a self-preserving mixing layer have been obtained by placing a trip wire near the origin of the flow (Batt, Kubota & Laufer 1970; Champagne, Pao & Wygnanski 1973) and it becomes questionable whether a universal self-preserving state actually exists or whether it can only be approached asymptotically for very large distances from the origin. The effect which the initial conditions have on the spread of the fully developed turbulent jet seems to be small; however no definitive statement can be made on the basis of the available data.

The results of Bradbury are also shown in figure 5, but they should not be compared with the others, because Bradbury's jet exhausted into a parallel stream which was moving at 0·16 of the jet exhaust velocity. In this case, although the conditions for self-preservation are not satisfied, it is nevertheless interesting to see the effect of the secondary stream on the growth of the jet.

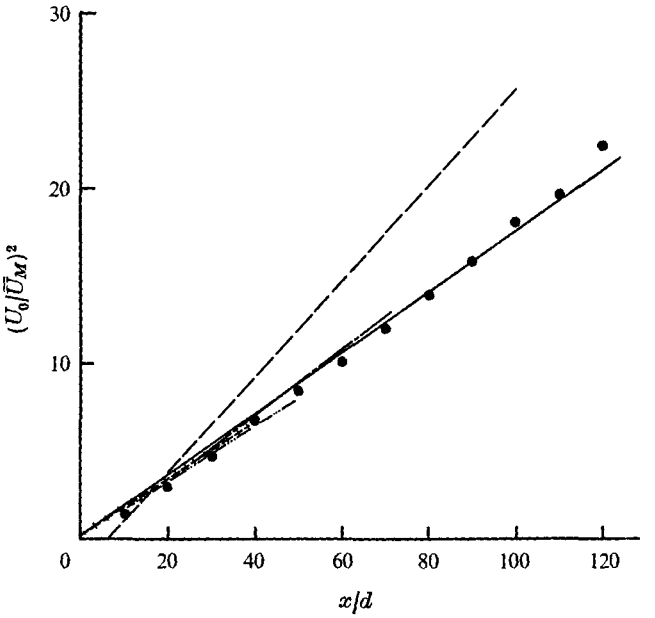

FIGURE 6. The decay of the mean velocity along the centre-line of the jet. Curves and symbols as in figure 5; $U_0(U_0-U_\infty)/(\overline{U}_M-U_\infty)^2$ is the ordinate variable for Bradbury's results.

The decay of the velocity scale $\overline{U}_M$ with x is given in figure 6, where U_0 is the velocity at the plane of the nozzle and $\overline{U}_M$ is the maximum velocity at a given x. In general, $\overline{U}_M \propto x^{-\frac{1}{2}}$; in Bradbury's case, however, momentum and similarity considerations yield

$$U_0(U_0-U_\infty)/(\overline{U}_M-U_\infty)^2 = 0{\cdot}188(x/d-3),$$

where U_∞ is the velocity of the external flow. This equation degenerates into the conventional decay law of a jet in quiescent surroundings as $U_\infty \to 0$. All the experimental results collapse onto a single universal curve with the exception of Heskestad's data. One may again speculate that the decay of the maximum velocity in the jet is somewhat dependent on the initial conditions. Table 1 provides a comparison of the various exit parameters reported. Of particular interest is the last column, which gives the ratio of the momentum of the jet at any cross-section to the momentum at the exit. These momenta were computed on the assumption that the pressure is constant across the jet and the velocity at the exit plane is uniform. The ratio J/J_0 is approximately 0·9 for a well-designed nozzle. The losses are attributed to the depletion of momentum in the internal boundary layers and a reduced pressure at the plane of the nozzle as a result of entrainment (Knystautas 1964; Wygnanski 1964). Bradbury's jet emerged from a nozzle which was located at the trailing edge of an airfoil, thus enabling the entrained streamlines to be approximately parallel to the axis of the jet and essentially eliminating the second cause of momentum loss. Hence in his case $J/J_0 = 0{\cdot}96$. The plane from which the jet emerged in the case of

Author(s)	$Re \times 10^{-4}$	d (in.)	Contraction	J/J_0†
Bradbury (1965)	3·0	0·375	2·67	0·96
Heskestad (1965)	3·4	0·500	2‡	0·611
Knystautas (1964)	4·1	0·245	24·5	0·93
Miller & Comings (1957)	1·78	0·500	56	0·87
Van der Hegge Zijnen (1958)	1·33	0·197	16	0·890
Present investigation	3·0	0·512	41·2	0·890

† $J = \rho \int_{-\infty}^{\infty} \overline{U}(\overline{U} - U_\infty)\, dy$; $J_0 = \rho U_0(U_0 - U_\infty)\, d$.

‡ The contraction is very rapid and resembles a thin orifice plate.

TABLE 1

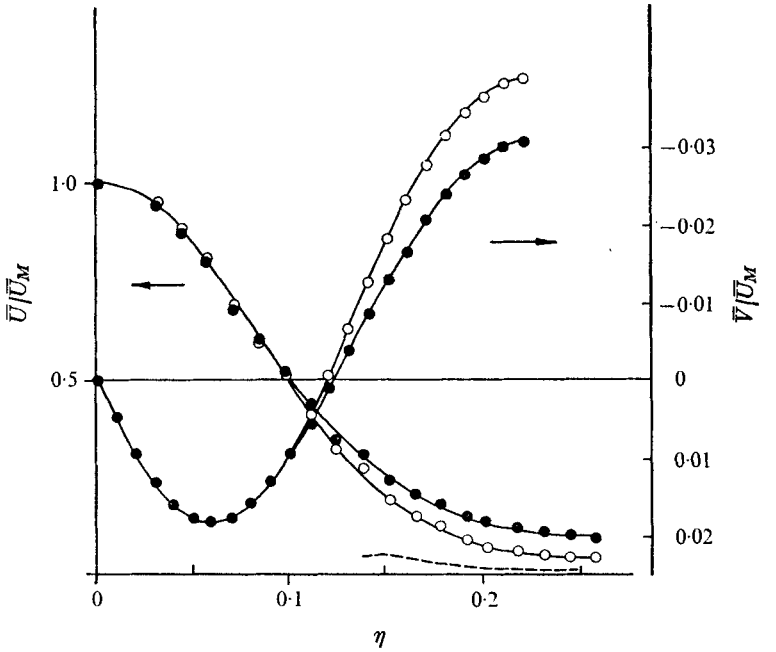

FIGURE 7. The conventional and turbulent zone-averaged velocities.
○, conventional; ●, turbulent zone; ---, irrotational zone.

Knystautas (1964) was barely one order of magnitude larger than the width of the orifice, contributing to a relatively large $J/J_0 = 0{\cdot}93$. The ratio of the momenta in Heskestad's experimental apparatus is exceptionally low, suggesting that the initial velocity profile is highly non-uniform; in fact the nozzle design resembles a thin orifice plate and the ratio $J/J_0 \simeq 0{\cdot}6$ is characteristic of an orifice discharge coefficient.

The mean velocity in the turbulent zone is identical to the conventional mean velocity for $\eta \leqslant 0{\cdot}1$ (i.e. as long as $\gamma = 1$) but is higher than the conventional mean velocity at the outer edge of the jet (figure 7). It has been observed that the fluid in the 'valleys' outside the turbulent zone is accelerated in the streamwise

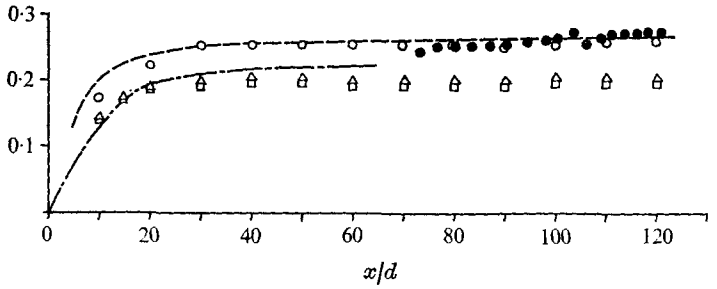

FIGURE 8. Variation of turbulent intensities along the centre-line of the jet. ○, ●, $\overline{(u'^2)}^{\frac{1}{2}}/\overline{U}_M$; △, $\overline{(v'^2)}^{\frac{1}{2}}/\overline{U}_M$; □, $\overline{(w'^2)}^{\frac{1}{2}}/\overline{U}_M$; — — —, $\overline{(u'^2)}^{\frac{1}{2}}/\overline{U}_M$, Bradbury (1965); ——, $\overline{(u'^2)}^{\frac{1}{2}}/\overline{U}_M$, Heskestad (1965).

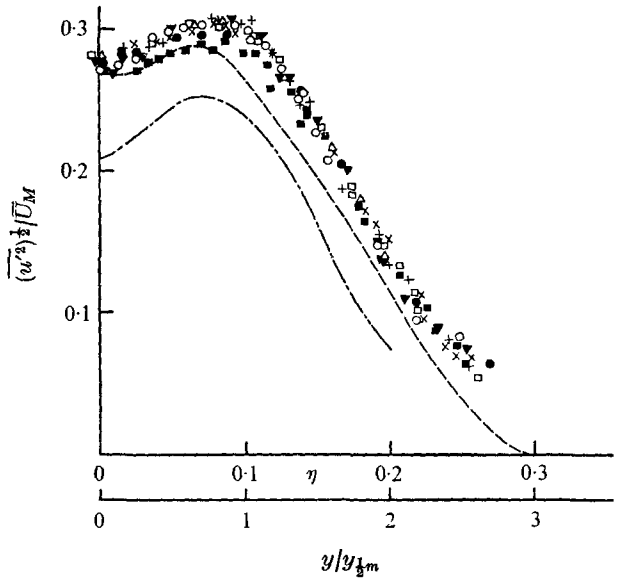

FIGURE 9. The conventional distribution of the axial velocity fluctuations. X-wire: ○, $x/d = 143$; △, $x/d = 129$; ▼, $x/d = 118$; □, $x/d = 106$; ●, $x/d = 95$. Normal hot wire: +, $x/d = 118$; ×, $x/d = 103$; ■, $x/d = 88$. ——, Heskestad (1965); — — —, Bradbury (1965).

direction by the turbulent bulges passing it. The velocity which the irrotational fluid acquires can be estimated from figure 7, by using the simple relation

$$\overline{U} = \overline{U}_T\gamma + \overline{U}_I(1-\gamma),$$

where the subscripts T and I refer to the turbulent and irrotational zones respectively.

The general relationship between the turbulent and irrotational zone-averaged velocities in a jet is similar to that at the outer edge of a mixing layer. In both instances it is the turbulent fluid which accelerates the ambient fluid. A quantitative comparison at the average location $\overline{Y}$ of the interface shows that

$$(\overline{U}_{Im}/\overline{U}_{IJ})_{\overline{Y}} = 2{\cdot}4, \quad (\overline{U}_m/\overline{U}_J)_{\overline{Y}} = 1{\cdot}85, \quad (\overline{U}_{Tm}/\overline{U}_{TJ})_{\overline{Y}} = 1{\cdot}67,$$

where the additional subscript m refers to the mixing layer and J refers to the jet.

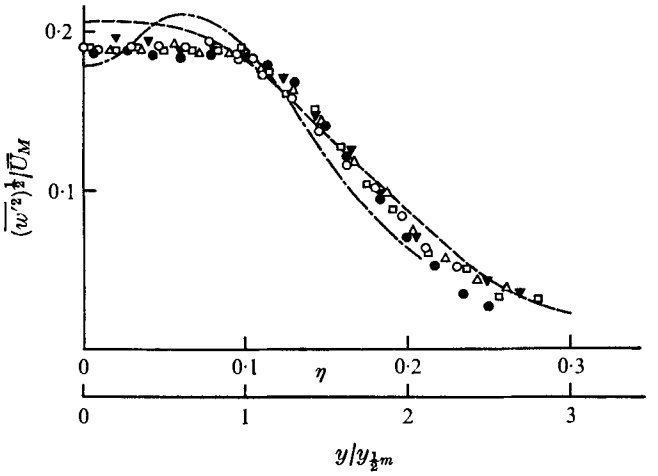

FIGURE 10. The conventional distribution of the transverse velocity fluctuations. ○, $x/d = 143$; △, $x/d = 129$; ▼, $x/d = 118$; □, $x/d = 106$; ●, $x/d = 95$. ——, Heskestad (1965); — — —, Bradbury (1965).

Thus when the velocities at the centre-plane or in the potential core of the two flows are equal the turbulent velocity at the interface of the mixing layer is higher than the turbulent velocity at the interface of the jet. The ratio between the corresponding potential velocities is even higher, implying that the mixing layer is capable of more vigorous momentum transfer from the turbulent zone to the surroundings than the fully developed jet. Figure 7 also shows the lateral velocities $\overline{V}$ and $\overline{V}_T$ calculated from the respective $\overline{U}$ profiles by applying continuity.

5. Fluctuation intensities and shear stress

The conventional r.m.s. values of the three components of the velocity fluctuations are shown in figures 8–11, while the turbulent shear stress is shown in figure 12. The measurements were made with X-wires, inclined single wires and normal wires. The results were corrected for finite turbulence levels by using the response equations derived by Heskestad (see equations 23–29, 36–39, 46 and 48 of his (1965) paper; all the correction terms inserted into those equations were measured).

The normalized turbulent intensities on the centre-plane of the jet attain their self-preserving state about 30 slot widths downstream from the nozzle (figure 8). The approach to self-preservation in a two-dimensional jet thus occurs much earlier than in an axisymmetric jet (Wygnanski & Fiedler 1969) or a two-dimensional wake (Townsend 1956, p. 138). In contrast to an axisymmetric jet there is no indication here that the transverse and lateral components $(\overline{w'^2})^{\frac{1}{2}}$ and $(\overline{v'^2})^{\frac{1}{2}}$ of the velocity fluctuations attain self-preservation long after the $(\overline{u'^2})^{\frac{1}{2}}$ component does. Bradbury (1965) estimated the distance necessary for self-preservation to be given by $x/d \geqslant 90$. He estimated this distance on the

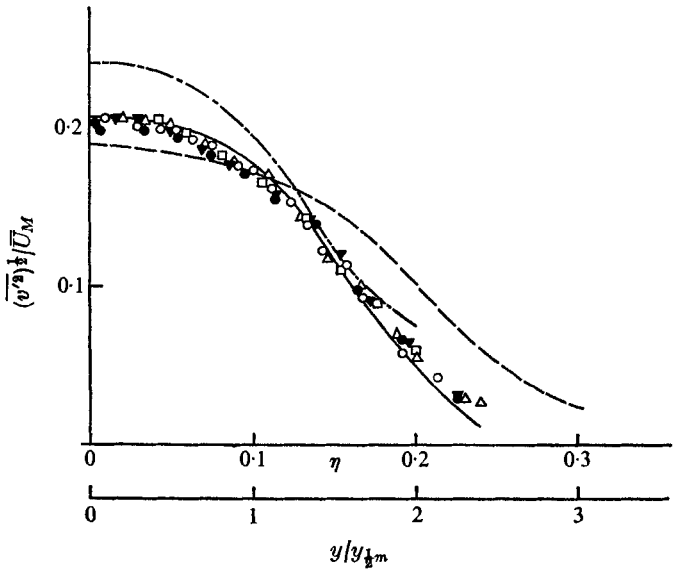

FIGURE 11. The conventional distribution of the lateral velocity fluctuations. X-wire: ○, $x/d = 143$; △, $x/d = 129$; ▼, $x/d = 118$; □, $x/d = 106$; ●, $x/d = 95$. — —, Heske stad (1965); ——, 45° hot wire; — — —, Bradbury (1965).

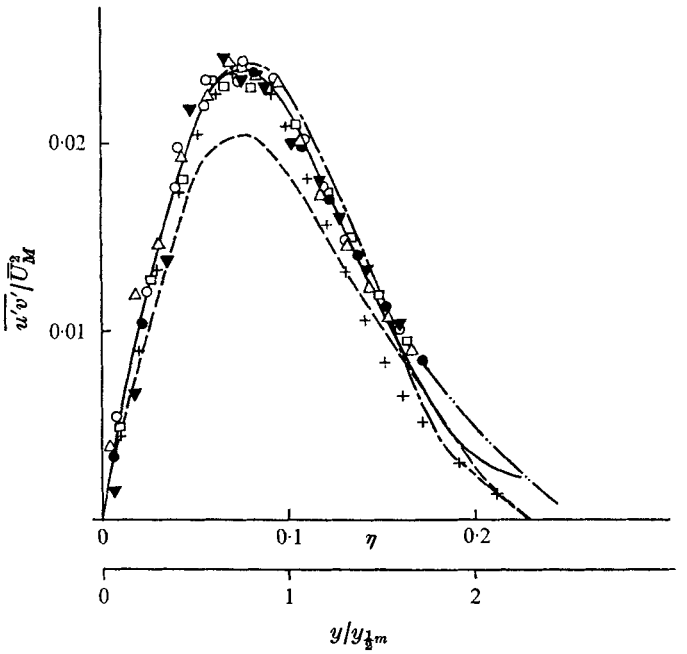

FIGURE 12. The conventional distribution of the turbulent shear stress. ——, calculated from mean velocity profile; —··—, 45° hot wire, corrected; +, 45° hot wire, not corrected. Other notation as in figure 11.

basis of Townsend's (1956) measurements in a wake. However his own findings agree rather well with the present results and the results of Heskestad (1965).

Two sets of measurements of $(\overline{u'^2})^{\frac{1}{2}}$ are shown in figure 8. This is because the apparatus was moved after two years to another location and some results were checked before this paper was written. No significant differences were observed as a consequence of the move. The results on the centre-plane are in good agreement with Heskestad's results in the region where self-preservation is expected. The $(\overline{u'^2})^{\frac{1}{2}}$ measurements reported by Bradbury are somewhat lower than the present values, implying the possibility that even a very small external velocity may have a profound effect on the state of self-preservation.

The magnitude of $(\overline{u'^2})^{\frac{1}{2}}$ along the centre-plane of the jet is higher than that of either $(\overline{v'^2})^{\frac{1}{2}}$ or $(\overline{w'^2})^{\frac{1}{2}}$ ($(\overline{w'^2})^{\frac{1}{2}}/(\overline{u'^2})^{\frac{1}{2}} = 0{\cdot}71$ and $(\overline{v'^2})^{\frac{1}{2}}/(\overline{u'^2})^{\frac{1}{2}} = 0{\cdot}82$) and thus any arguments for complete isotropy even in the absence of local shear can not be considered seriously. Anisotropy was observed in all other free shear flows which were investigated and the two-dimensional jet is no exception.

The intensity profiles measured by Heskestad and Bradbury, as well as here, are compared in figures 9–11. The $(\overline{u'^2})^{\frac{1}{2}}$ profile of Heskestad compares favourably with the profile that we have measured. The profile of Bradbury (although compared on the basis of $y/y_{\frac{1}{2}m}$ rather than η) is still much narrower and has a strong peak at $y/y_{\frac{1}{2}m} = 0{\cdot}8$. The intensity of this peak relative to the intensity at the centre is indicative of a lack of self-preservation.

Turbulence is not generally capable of adjusting itself quickly to local conditions, and so the termination of the irrotational core, some 5–10 characteristic nozzle dimensions downstream of the orifice, may still have an effect on the flow far downstream. The turbulent intensity resulting from the merging of the two mixing layers has a very strong saddle shape, which slowly disappears with increasing x. Thus, the larger the ratio $\overline{u'^2_{\max}}/\overline{u'^2_{\text{centre}}}$ the stronger is the indication that the measurements were made too close to the nozzle. In an axisymmetric jet (Wygnanski & Fiedler 1969) the distribution of $(\overline{u'^2})^{\frac{1}{2}}$ had a saddle shape whenever the measurements were made at $x/d \leqslant 30$. A similar peak is shown by Bradbury in the $(\overline{w'^2})^{\frac{1}{2}}$ profile.

In the central core of the jet Bradbury observed a $(\overline{u'^2})^{\frac{1}{2}}$ profile 25 % lower than those observed by Heskestad and by us, a $(\overline{w'^2})^{\frac{1}{2}}$ profile approximately identical to ours and a $(\overline{v'^2})^{\frac{1}{2}}$ profile 15 % higher. The agreement between Heskestad's results and ours is fairly good for $\eta < 0{\cdot}1$. For $\eta > 0{\cdot}1$, however, Heskestad's $(\overline{u'^2})^{\frac{1}{2}}$ profile is consistently lower than ours, his $(\overline{w'^2})^{\frac{1}{2}}$ profile agrees well but his $(\overline{v'^2})^{\frac{1}{2}}$ profile is significantly higher. One may attribute the differences to the prevailing direction of the entrainment field and the strength of the room draughts.

The measured distribution of the turbulent shear stress $\overline{u'v'}$ is compared with the distribution calculated from the corrected mean velocity profile by neglecting the normal stresses in figure 12. The agreement between the two is excellent. The shear-stress distribution also agrees very well with Bradbury's measurements but is higher than Heskestad's. It should be pointed out that Heskestad's measured values of $\overline{u'v'}$ do not agree with his calculations. In the

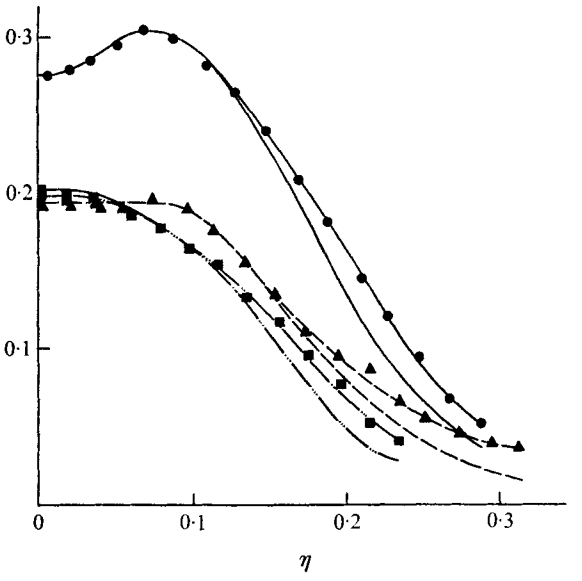

FIGURE 13. The conventional (curves) and turbulent zone-averaged (symbols) distributions of the three components of the turbulence intensity. ——, ●, $(\overline{u'^2})^{\frac{1}{2}}/\overline{U}_M$; — —, ▲, $(\overline{w'^2})^{\frac{1}{2}}/\overline{U}_M$; —···—, ■, $(\overline{v'^2})^{\frac{1}{2}}/\overline{U}_M$.

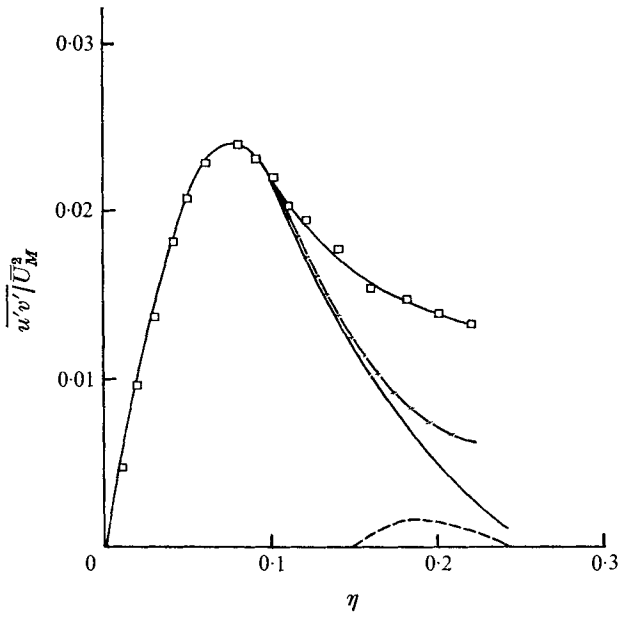

FIGURE 14. The conventional and zone-averaged distributions of the turbulent shear stress. ——, conventional; □, turbulent zone; – – – –, irrotational zone; —×—, calculated from turbulent-zone mean velocity profile.

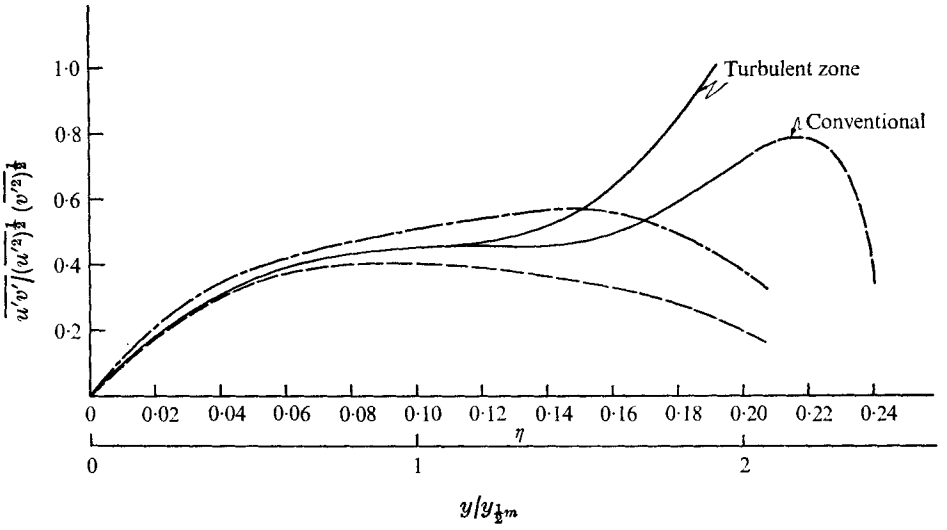

FIGURE 15. Variation of the shear-stress correlation across the jet. ——, present measurements; — — —, Bradbury (1965); — —, Heskestad (1965).

axisymmetric jet the calculated shear stress agrees well with the measurements of $\overline{u'v'}$ but in the mixing layer (Wygnanski & Fiedler 1970) the calculated shear is in error and there is actually a discrepancy of about 20 % between the data and the calculations. Since there is some question as to the accuracy of DISA X-wires (Jerome, Guitton & Patel 1971) the experiments were repeated using a single inclined wire. The results were identical and are compared in figures 11 and 12. From figure 12 one may also estimate the importance of correcting the hot-wire response equations for large intensities. The differences are significant for $\eta > 0{\cdot}1$.

The turbulent zone-averaged intensities are compared in figure 13 with the conventional distributions of these intensities. The trend is very similar to that observed in a mixing layer, namely the turbulent zone averages become high in comparison with the conventional averages at the outer extremes of the jet. Also, the distribution of $(\overline{u'v'})_T$ is very high in comparison with the conventionally measured distribution of $\overline{u'v'}$ at the same η for $\eta > 0{\cdot}15$ (figure 14). This indicates that in the irrotational valleys $(\overline{u'v'})_I$ is very small (figure 14). The lack of irrotational fluctuations gives the $\overline{u'v'}$ trace a very strongly burst-like appearance in the outer region of the jet (see also Wygnanski & Fiedler 1969, figure 10).

The shear stress computed from $\overline{U}_T$ does not agree with the measured values of $(\overline{u'v'})_T$. The shear-stress correlation in the turbulent zone (figure 15) approaches unity at $\eta = 0{\cdot}2$ while the conventional value is still less than 0·7. It is interesting to note that the correlations measured by Heskestad and Bradbury drop at $\eta > 0{\cdot}15$ while the correlation measured by us increases monotonically with increasing η.

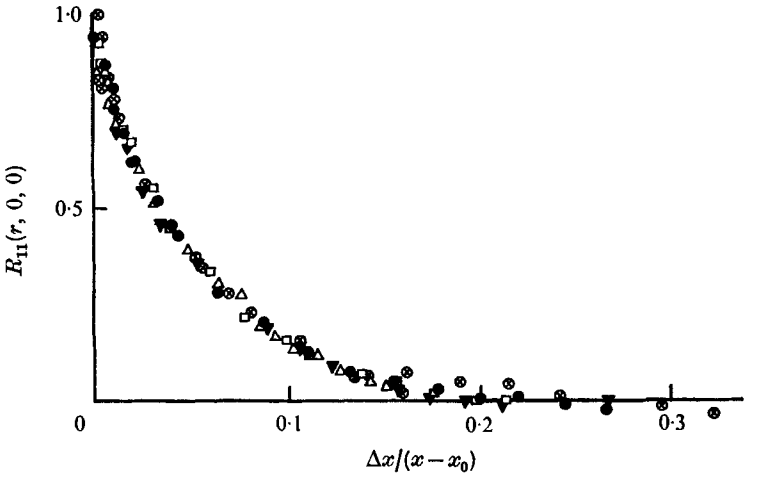

FIGURE 16. The longitudinal correlation along the centre-plane of the jet. $\Lambda_f = 0{\cdot}0479x$. ⊗, $x/d = 78$; ●, $x/d = 93$; □, $x/d = 105$; ▼, $x/d = 116$; △, $x/d = 128$.

6. Two-point velocity correlations

The longitudinal correlation coefficient at any point in the jet is defined by

$$R_{11}(r,0,0) = \frac{\overline{u'(x+\frac{1}{2}\Delta x)\,u'(x-\frac{1}{2}\Delta x)}}{[\overline{u'^2(x+\frac{1}{2}\Delta x)}]^{\frac{1}{2}}\,[\overline{u'^2(x-\frac{1}{2}\Delta x)}]^{\frac{1}{2}}}$$

and the lateral correlation coefficient by

$$R_{11}(0,r,0) = \frac{\overline{u'(y+\frac{1}{2}\Delta y)\,u'(y-\frac{1}{2}\Delta y)}}{[\overline{u'^2(y+\frac{1}{2}\Delta y)}]^{\frac{1}{2}}\,[\overline{u'^2(y-\frac{1}{2}\Delta y)}]^{\frac{1}{2}}}.$$

This definition alleviates a little the difficulty of defining the point relative to which the correlation is measured in non-homogeneous flow.

The distribution of $R_{11}(r,0,0)$ along the axis of the jet (figure 16) indicates that the large-scale structure grows linearly with x, i.e. that the flow is self-preserving. The ratio $\Lambda_f/y_{\frac{1}{2}m}$ of the integral scale

$$\Lambda_f = \int_0^\infty R_{11}(r,0,0)\,dx$$

to the width of the jet is equal to 0·47 for the two-dimensional jet and 0·45 for the axisymmetric jet (Wygnanski & Fiedler 1969). The lateral integral scales $\Lambda_g/y_{\frac{1}{2}m}$ of the two flows are also in reasonably good agreement, implying that the gross behaviour of the two jets is similar in spite of the differences in geometry. (Only the positive area under the $R_{11}(0,r,0)$ correlation curve (figure 17) was considered in computing Λ_g.)

A closer examination of the correlations in the two flows shows some marked differences.

(i) The negative dip in the $R_{11}(0,r,0)$ correlation in the two-dimensional jet is stronger than that in the axisymmetric jet and extends to $\Delta y/(x-x_0) = 0{\cdot}3$.

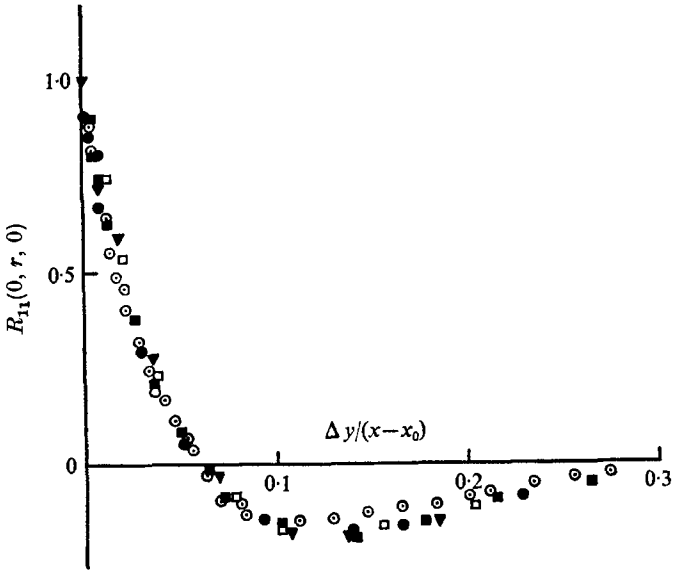

FIGURE 17. The lateral correlation along the centre-plane of the jet. $\Lambda_g = 0{\cdot}0219x$. ▼, $x/d = 116$; □, $x/d = 105$; ●, $x/d = 95$; ■, $x/d = 81$; ○, $x/d = 70$.

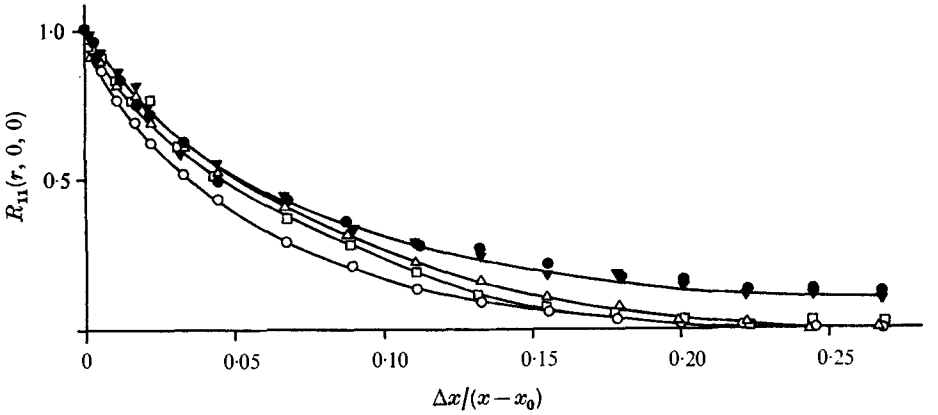

FIGURE 18. Variation of the longitudinal correlation across the jet. $x/d = 93$.

	○	△	▼	●	□
Λ_f/x	0·0479	0·0702	0·0889	0·0876	0·0606
η	0	0·05	0·10	0·15	0·20

In the axisymmetric jet $R_{11}(0,r,0)$ vanishes for $\Delta y/(x-x_0) > 0{\cdot}12$, but this is not so in the two-dimensional jet. In other words, the large eddies are preserved longer in the two-dimensional configuration. This is hardly surprising because velocity perturbations decay more slowly in the two-dimensional jet than in the axisymmetric jet.

(ii) Both the integral scales Λ_f and Λ_g increase monotonically with η in the axisymmetric jet. However, the rate of increase $d\Lambda_f/d\eta$ becomes smaller at the

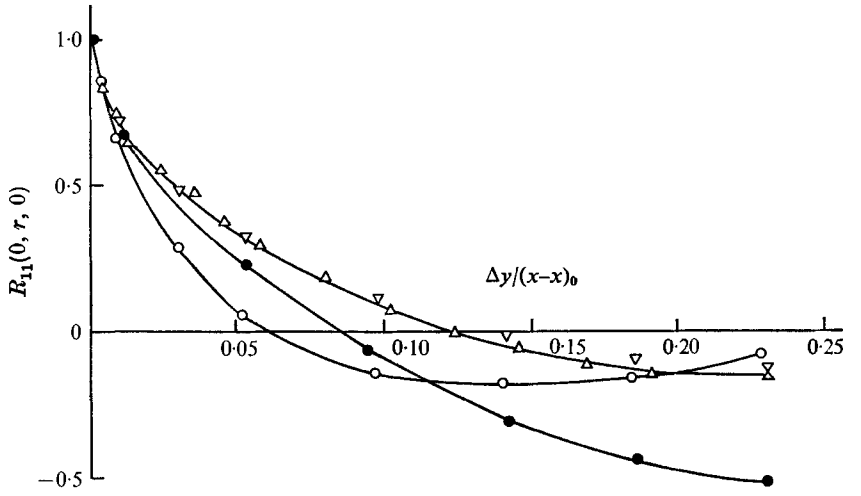

FIGURE 19. Variation of the lateral correlation across the jet. $x/d = 93$.

	○	△	▽	●
Λ_g/x	0·0219	0·0414	0·0414	0·0304
η	0	0·05	0·10	0·15

edge of the jet. In the two-dimensional flow the integral scales attain a maximum at $\eta \simeq 0{\cdot}1$ and then decrease with increasing η. (See figures 18 and 19.)

(iii) The negative dip in the $R_{11}(0, r, 0)$ correlation curves in the axisymmetric jet disappears at $\eta > 0{\cdot}05$ (Wygnanski & Fiedler, 1969, figure 16), while the $R_{11}(0, r, 0)$ correlations in the present flow exhibit an even more negative correlation with increasing η. At $\eta = 0{\cdot}15$ the value $R_{11}(0, r, 0) = -0{\cdot}5$ was observed at $\Delta y/(x - x_0) = 0{\cdot}23$.

One may compare the standard deviation σ of the interface from its mean location $\overline{Y}$ with the lateral integral scale Λ_g. The ratio σ/Λ_g was observed to be approximately unity at $y = \overline{Y}$ in all the turbulent shear flows considered, which means that the interface is primarily contorted by the lateral large-scale eddies.

The value of Λ_f deduced from integrating the $R_{11}(r, 0, 0)$ correlation was compared for two locations in the flow with the value of Λ_f calculated from the one-dimensional power spectrum $E_1(k)$, i.e. from

$$\Lambda_f = \tfrac{1}{2}\pi[E_1(0)/\overline{u'^2}].$$

The two results were within 5 % of one another.

7. Dissipation terms and microscales

Three temporal derivatives were measured in order to estimate the dissipation term in the energy equation. Previous experience enabled us to take one short cut, namely to use Heskestad's (1965) transformation from temporal to spatial derivatives without the necessity of measuring the convection velocity of the dissipation scales (see Wygnanski & Fiedler 1970, figure 23).

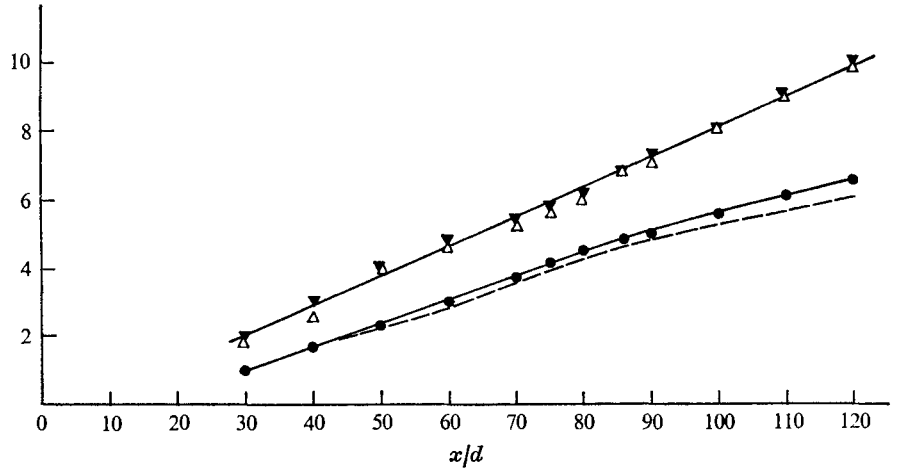

FIGURE 20. The dissipation terms along the centre-plane of the jet.

———, $\overline{\left(\frac{\partial u'}{\partial x}\right)^2}\frac{x\nu}{\overline{U}_M^3} \times 10^3$, Heskestad (1965).

Present results: ●, $\overline{\left(\frac{\partial u'}{\partial x}\right)^2}\frac{x\nu}{\overline{U}_M^3} \times 10^3$; ▼, $\overline{\left(\frac{\partial w'}{\partial x}\right)^2}\frac{x\nu}{\overline{U}_M^3} \times 10^3$; △, $\overline{\left(\frac{\partial v'}{\partial x}\right)^2}\frac{x\nu}{\overline{U}_M^3} \times 10^3$.

No wire-length corrections were applied to the data because it was estimated that the attenuation of the temporal derivatives was small ($4 \leqslant l_w/\eta_k \leqslant 12$, where η_k is the Kolmogorov microscale and l_w is the length of the wire). Wyngaard (1969) has shown that 90 % response to $\overline{(\partial u'/\partial x)^2}$ is obtained provided that $l_w \leqslant 4\eta_k$. A detailed discussion of this point was also given by Champagne *et al.* (1973).

The dissipation terms increase almost linearly with x along the centre-plane of the jet (figure 20). The lateral and transverse derivatives $\overline{(\partial v'/\partial x)^2}$ and $\overline{(\partial w'/\partial x)^2}$ are almost equal while $\overline{(\partial u'/\partial x)^2}$ is much lower than both. However the isotropic relation

$$\overline{(\partial v'/\partial x)^2} = 2\overline{(\partial u'/\partial x)^2}$$

does not hold everywhere in the jet. Isotropic relations do seem to hold close to the exit, where most probably the jet is not yet fully self-preserving. The agreement with the values of $\overline{(\partial u'/\partial x)^2}$ measured by Heskestad is very good. In order to make the comparison $\overline{U}_M^2\overline{(\partial u'/\partial t)^2}$ was taken from figure 20 of Heskestad's paper and multiplied by the factor $x\nu/(\overline{U}_M^2 + \overline{u'^2} + 2\overline{v'^2} + \overline{w'^2})\overline{U}_M$, which was again deduced from his 1965 paper. The increase in the dissipation terms with x signifies that the total turbulent energy budget will also change with x. Furthermore the lateral profiles of the dissipation terms are not similar even for $x/d > 100$ (see figures 21 and 22). In the outer region of the jet ($\eta > 0{\cdot}13$) the conventionally averaged dissipation terms are all approximately equal and almost independent of x. The turbulent zone averages on the other hand vary with x across the entire jet (figure 22). In the central region of the jet there is a tendency towards isotropy, with $\overline{(\partial v'/\partial x)^2}$ and $\overline{(\partial w'/\partial x)^2}$ increasing much faster than $\overline{(\partial u'/\partial x)^2}$ as η decreases. The turbulent zone averages of $\overline{(\partial u'/\partial x)^2}$ are almost constant across the jet.

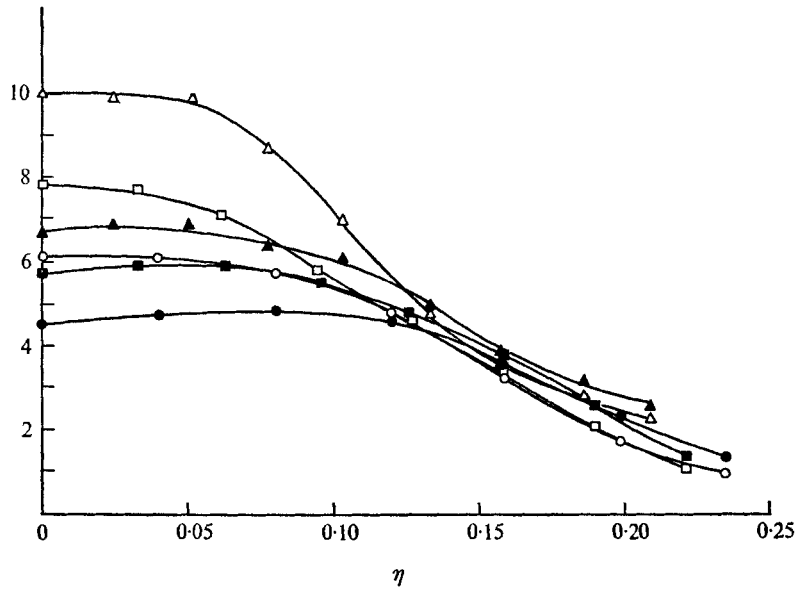

FIGURE 21. Conventional lateral profiles of the dissipation terms. $\overline{\left(\frac{\partial u'}{\partial x}\right)^2}\frac{xv}{\overline{U}_M^3}\times 10^3$: ▲, $x/d = 120$; ■, $x/d = 100$; ●, $x/d = 80$. $\overline{\left(\frac{\partial v'}{\partial x}\right)^2}\frac{xv}{\overline{U}_M^3}\times 10^3$, $\overline{\left(\frac{\partial w'}{\partial x}\right)^2}\frac{xv}{\overline{U}_M^3}\times 10^3$: △, $x/d = 120$; □, $x/d = 100$; ○, $x/d = 80$.

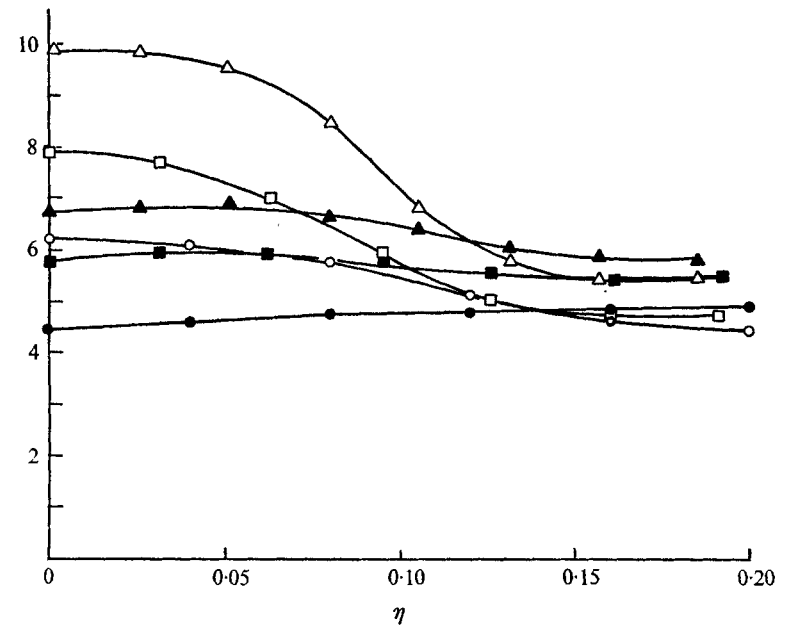

FIGURE 22. Lateral profiles of the dissipation terms in the turbulent zone. Symbols as in figure 21.

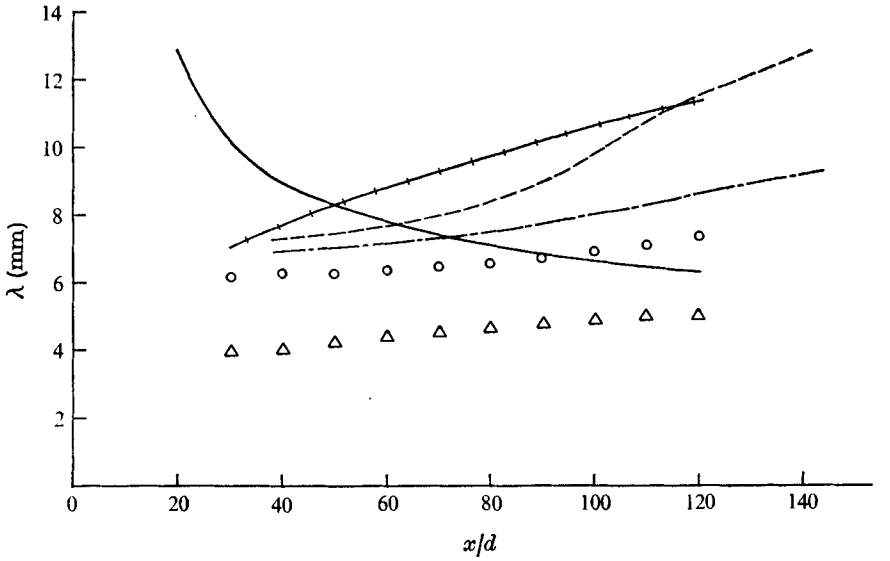

FIGURE 23. Variation of the microscales along the jet centre-plane, — —, Heskestad (1965); — – —, Heskestad (1965), calculated from $\overline{(\partial u'/\partial t)^2}/\overline{U}_M^2$; ——, $Re_T = [\overline{(u'^2)}^{\frac{1}{2}}\lambda_g/\nu] \times 10^{-2}$; ⊣⊢⊣⊢, $(\nu^3/\epsilon)^{\frac{1}{4}} \times 10^2$; ○, λ_f; △, λ_g.

The microscales λ_f and λ_g, defined by

$$\lambda_f^2 = 2\overline{(u')^2}\Big/\overline{\left(\frac{\partial u'}{\partial x}\right)^2}, \quad \lambda_g^2 = 2\overline{(v')^2}\Big/\overline{\left(\frac{\partial v'}{\partial x}\right)^2},$$

increase very slowly with distance from the nozzle (figure 23). λ_f is almost constant for $x/d \leqslant 80$ while λ_g increases linearly with x for $x/d \geqslant 30$. The rate of increase of λ_g with x is given by

$$[\partial\lambda_g/\partial x]_{\eta=0} = 9 \times 10^{-4}.$$

Exceptionally large values, as far as laboratory flows are concerned, of the turbulent Reynolds number $Re_T \equiv \overline{(u'^2)}^{\frac{1}{2}}\lambda_g/\nu$ were obtained in the two-dimensional jet (figure 23). This is because the absolute value of u' initially increased rapidly with x while λ_g was almost independent of this co-ordinate. The two-dimensional jet is thus very suitable for investigating the proposition of local isotropy. In most laboratory flows known to the authors $Re_T \simeq 800$ while here it attained 1000 (Grant, Stewart & Moilliet 1962 measured $Re_T = 2000$ in Discovery Passage off Vancouver Island). The Kolmogorov length scale $(\nu^3/\epsilon)^{\frac{1}{4}}$ on the centre-plane of the jet is also shown in figure 23; ϵ is the viscous dissipation term.

In order to compare the present measurements of microscales with Heskestad's some manipulation is required because Heskestad defined

$$\lambda_f \equiv \frac{\overline{(q'^2)}^{\frac{1}{2}}}{\sqrt{3}}\Big/\left[\overline{\left(\frac{\partial u'}{\partial x}\right)^2}\right]^{\frac{1}{2}},$$

where $$\overline{(q'^2)}^{\frac{1}{2}} = (\overline{u'^2} + \overline{v'^2} + \overline{w'^2})^{\frac{1}{2}},$$

and thus $$\lambda_f^2 = (\lambda_f^2)_{\text{Heskestad}}\, 6\overline{(u')^2}/\overline{q'^2}.$$

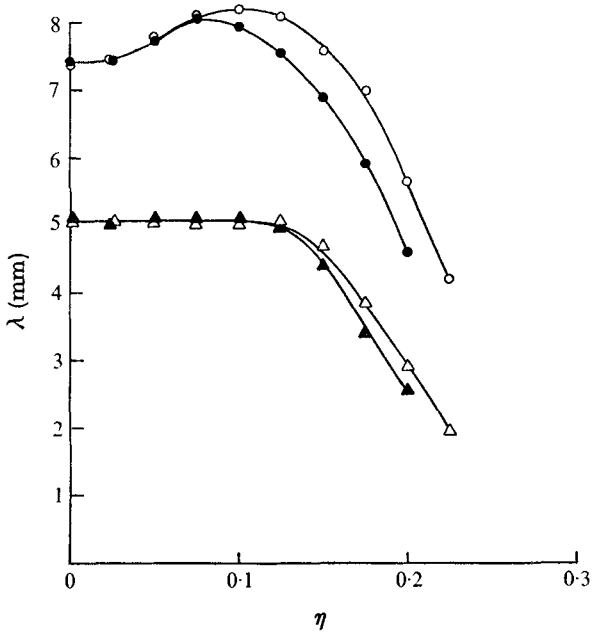

FIGURE 24. Distribution of microscales across the jet. ○, λ_f, conventional; ●, λ_f, turbulent zone; △, λ_g, conventional; ▲, λ_g, turbulent zone.

The two dashed lines shown in figure 23 represent Heskestad's results. The top line was taken from figure 33 of his paper and multiplied by the appropriate factor; the bottom line was calculated directly from his figure 20 and agrees better with the present data. One may be puzzled at first to discover that in spite of the good agreement between Heskestad's results for $(\overline{u'^2})^{\frac{1}{2}}/\overline{U}_M$ and $\overline{(\partial u'/\partial x)^2}$ at the centre of the jet and our own (figures 8 and 23) there is a difference in the values of λ_f. The discrepancy results from a different decay of the mean velocity with x. By plotting $\overline{U}_M\lambda_f/\nu$ as the ordinate in figure 23 instead of λ_f the differences are mostly reconciled.

The microscales decline in value towards the outer part of the jet (figure 24). This decline occurs for $\eta \geqslant 0{\cdot}1$, while for $0 \leqslant \eta \leqslant 0{\cdot}1$ no microscale measured changes with η. This is in contrast to the observations made in the axisymmetric jet (Wygnanski & Fiedler 1969), where some microscales increased with η.

8. Higher-order correlations and turbulent energy budget

The six triple velocity products (figures 25–27) and some fourth-order products (figure 28) were measured in order to evaluate the budget of turbulent energy and to ascertain the corrections to hot-wire readings resulting from the high turbulent intensities which occur in this flow. The conventionally measured correlations vanish at the centre of the jet, attaining a maximum around $\eta = 0{\cdot}1$, and decline to zero at the outer edge. A minor exception is the small negative dip in the $\overline{u'^2v'}$ correlation for $0 \leqslant \eta \leqslant 0{\cdot}035$. The negative value of $\overline{u'^2v'}$ results

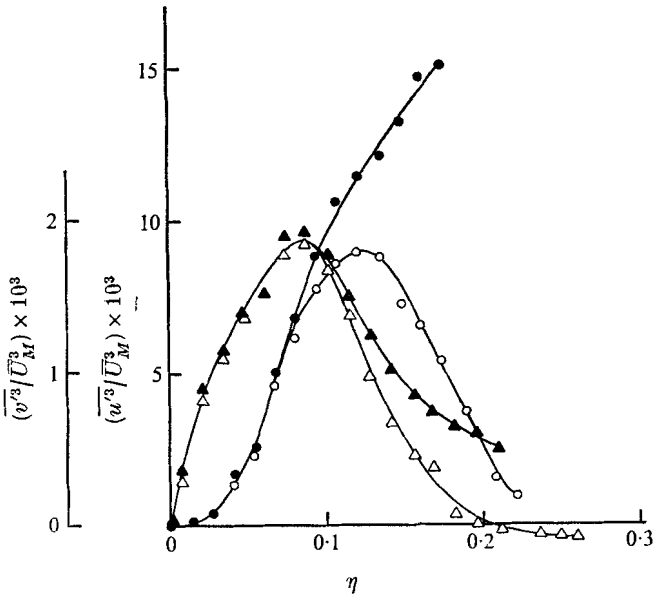

FIGURE 25. Conventional (open symbols) and turbulent-zone (solid symbols) triple velocity products. ○, $\overline{(u'^3}/\bar{U}_M^3) \times 10^3$; △, $\overline{(v'^3}/\bar{U}_M^3) \times 10^3$.

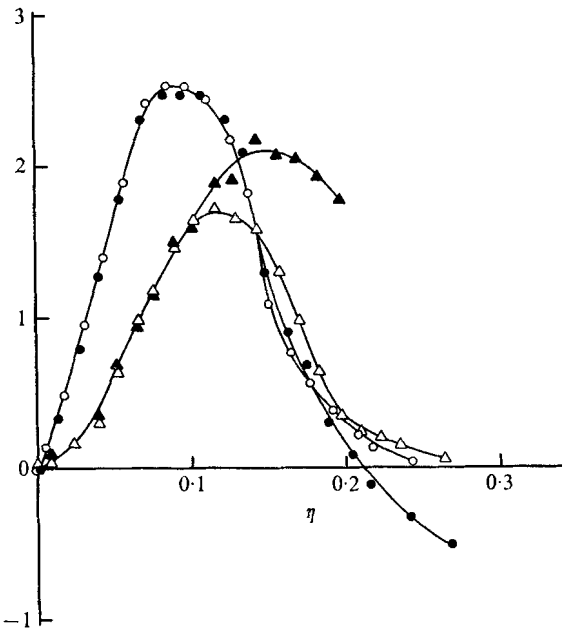

FIGURE 26. Conventional (open symbols) and turbulent-zone (solid symbols) triple velocity products. ○, $\overline{(u'v'^2}/\bar{U}_M^3) \times 10^3$; △, $\overline{(u'w'^2}/\bar{U}_M^3) \times 10^3$.

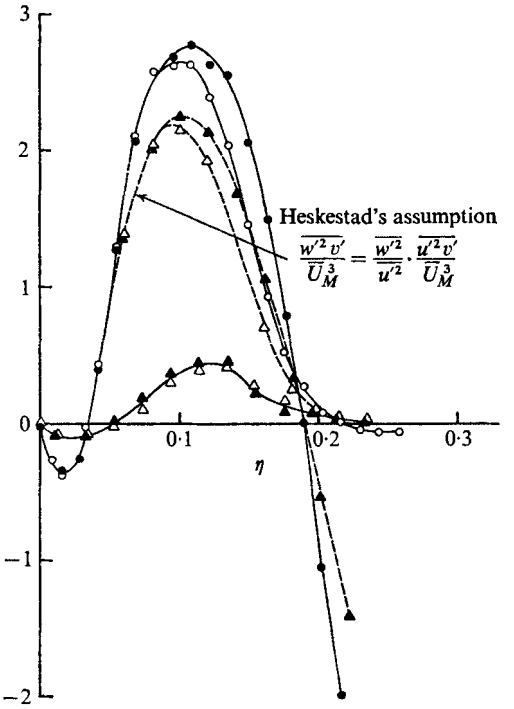

FIGURE 27. Conventional (open symbols) and turbulent-zone (solid symbols) triple velocity products. ○, $(\overline{u'^2v'}/\overline{U}_M^3) \times 10^3$; △, $(\overline{w'^2v'}/\overline{U}_M^3) \times 10^3$.

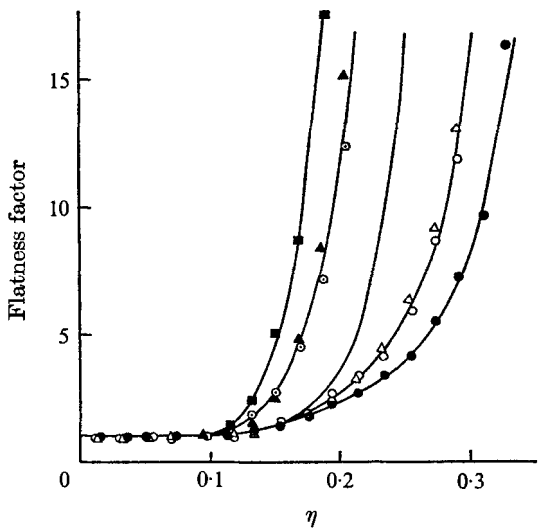

FIGURE 28. The flatness factors. ——, $1/\gamma$. Symbols denote the following quantities normalized by their centre-plane values:

■, $\overline{\left(\frac{\partial u'}{\partial x}\right)^4} \Big/ \left[\overline{\left(\frac{\partial u'}{\partial x}\right)^2}\right]^2$; ⊙, $\overline{\left(\frac{\partial v'}{\partial x}\right)^4} \Big/ \left[\overline{\left(\frac{\partial v'}{\partial x}\right)^2}\right]^2$; ▲, $\overline{\left(\frac{\partial w'}{\partial x}\right)^4} \Big/ \left[\overline{\left(\frac{\partial w'}{\partial x}\right)^2}\right]^2$;

●, $\frac{\overline{u'^4}}{(\overline{u'^2})^2}$; ○, $\frac{\overline{v'^4}}{(\overline{v'^2})^2}$; △, $\frac{\overline{w'^4}}{(\overline{w'^2})^2}$.

from the fact that $\overline{u'^2}$ peaks at positive η and some diffusion of u'^2 towards the centre of the jet occurs.

Rather different results are observed for some turbulent-zone triple products, particularly $\overline{(u')^3_T}$ and $\overline{(u'^2v')_T}$. The value of $\overline{(u')^3_T}$ increases monotonically with η while $\overline{(u'^2v')_T}$ becomes negative for $\eta > 0{\cdot}2$, i.e. neither quantity drops to zero at the edge of the turbulent region of the jet; since turbulent zone averages become of the form 0/0 as $\gamma \to 0$, non-zero values at very large η are not impossible. The very same behaviour was observed on the low velocity side of the two-dimensional mixing layer.

The triple correlation $\overline{v'w'^2}$ was measured using the method of Townsend (1949). The results appear to be smaller than was expected since the ratio $(\overline{v'u'^2})_{\max}/(\overline{v'w'^2})_{\max} \simeq 6$. In the two-dimensional mixing layer and in the axisymmetric jet $2 < (\overline{v'u'^2})_{\max}/(\overline{v'w'^2})_{\max} < 3$.

Heskestad (1965) did not measure $\overline{v'w'^2}$ but assumed that

$$\frac{\overline{v'w'^2}}{\overline{U}_M^3} = \frac{\overline{w'^2}}{\overline{u'^2}}\frac{\overline{v'u'^2}}{\overline{U}_M^3};$$

the same assumption is also made here and the results shown in figure 27 for comparison.

In figure 28 lateral distributions of flatness factors are shown. The results were normalized by the flatness factors at the centre of the jet and hence should represent some measure of the reciprocal γ^{-1} of the intermittency. The flatness factors of the derivative signals indicate a narrower distribution of γ^{-1} than was actually measured, while the flatness factors of the signals themselves indicate a wider distribution of γ^{-1}. The inherent subjectivity in determining γ from one or two components of the velocity fluctuation is apparent in this figure. By using the derivatives only, one gravitates towards the higher frequencies and hence more stringent requirements are set for the decision that the flow is turbulent. The use of the signal itself brings in some low frequencies which may or may not belong to the turbulent flow. The situation is further complicated by the fact that the flatness factors of the v' and w' components do not have the same distribution as the flatness factor of the u' component. It may also be noted that the flatness factors of u' and its temporal derivative are further apart than the flatness factors of v' and its derivative.

The energy equation is written in the form

$$\underbrace{\left\{\frac{1}{2}\left[\frac{\partial}{\partial\eta}\left(\frac{\overline{q'^2}}{\overline{U}_M^2}\right)\right]\left(\frac{\overline{V}}{\overline{U}_M} - \eta\frac{\overline{U}}{\overline{U}_M}\right) - \frac{1}{2}\frac{\overline{q'^2}}{\overline{U}_M^2}\frac{\overline{U}}{\overline{U}_M}\right\}}_{\text{Convection}} + \underbrace{\left\{\frac{1}{2}\frac{\partial}{\partial\eta}\left(\frac{\overline{v'q'^2}}{\overline{U}_M^3}\right) - \tfrac{1}{2}\eta\frac{\partial}{\partial\eta}\left(\frac{\overline{u'q'^2}}{\overline{U}_M^3}\right) - \frac{3}{4}\frac{\overline{u'q'^2}}{\overline{U}_M^3}\right\}}_{\text{Diffusion}}$$

$$\underbrace{-\left[\eta\frac{\partial}{\partial\eta}\frac{\overline{p'u'}}{\rho\overline{U}_M^3} - \frac{\partial}{\partial\eta}\frac{\overline{p'v'}}{\rho\overline{U}_M^3} + \frac{3}{2}\frac{\overline{u'p'}}{\rho\overline{U}_M^3}\right]}_{\text{Pressure transport}} + \underbrace{\left\{\frac{\overline{u'v'}}{\overline{U}_M^2}\frac{\partial}{\partial\eta}\left(\frac{\overline{U}}{\overline{U}_M}\right) - \left(\frac{\overline{u'^2}}{\overline{U}_M^2} - \frac{\overline{v'^2}}{\overline{U}_M^2}\right)\left[\eta\frac{\partial}{\partial\eta}\left(\frac{\overline{U}}{\overline{U}_M}\right) + \frac{1}{2}\frac{\overline{U}}{\overline{U}_M}\right]\right\}}_{\text{Production}}$$

$$\underbrace{+\frac{x}{\overline{U}_M^3}\epsilon}_{\text{Dissipation}} = 0.$$

In deriving this equation self-preservation was assumed and the boundary-layer approximation was used for the mean velocity profile. The viscous diffusion term was found to be negligible and the viscous dissipation was assumed to be

$$\frac{x}{\overline{U}_M^3}\epsilon = 15\frac{x\nu}{\overline{U}_M^3}\overline{\left(\frac{\partial u'}{\partial x}\right)^2}.$$

Although we realize that the isotropic assumption for the dissipation term does not hold very well it was used here for two reasons.

(i) Since it is very difficult to measure all the derivatives comprising the dissipation term, the isotropic assumption is probably as good as any. In a previous paper (Wygnanski & Fiedler 1969) a 'semi-isotropic' assumption was made because the isotropic relations held only on the centre-line of the jet. Away from the centre

$$\overline{\left(\frac{\partial v'}{\partial x}\right)^2}\Big/\overline{\left(\frac{\partial u'}{\partial x}\right)^2} < 2 \quad \text{while} \quad \overline{\left(\frac{\partial u'}{\partial y}\right)^2}\Big/\overline{\left(\frac{\partial u'}{\partial x}\right)^2} > 2$$

and the two ratios might have compensated one another so as to yield on the average

$$4\overline{\left(\frac{\partial u'}{\partial x}\right)^2} = \overline{\left(\frac{\partial v'}{\partial x}\right)^2} + \overline{\left(\frac{\partial u'}{\partial y}\right)^2}.$$

(ii) The dissipation yielded by the isotropic assumption is very nearly that required to make the integral of the diffusion term (obtained by difference) equal to zero, as it should be. If one assumes that

$$\epsilon = 3\nu\left[\overline{\left(\frac{\partial u'}{\partial x}\right)^2} + \overline{\left(\frac{\partial v'}{\partial x}\right)^2} + \overline{\left(\frac{\partial w'}{\partial x}\right)^2}\right]$$

the dissipation term is 20–30 % lower. The pressure-transport term, which makes the largest contribution to the diffusion, becomes too large and the integral of the total diffusion across the flow does not vanish. Bradbury (1965) scaled up his measured dissipation term to ensure that the net diffusion across the jet was indeed zero. He used the same isotropic relations yet he claimed that his hot wire did not have a sufficient frequency response or spatial resolution in order to measure the dissipation correctly. Heskestad's results for the diffusion term, although qualitatively in agreement with ours, do not seem to integrate to zero across the jet.

The terms in the energy equation were computed from the data at $x/d = 120$ and are shown in figures 29–31. The energy budget in the turbulent zone should be regarded as an average budget for the interior of the turbulent bulges. A more representative budget could be obtained if the acquisition of the data excluded all thin layers near the interfaces; at the time this was not possible and consequently the results presented here can be taken as valid for the interior of the turbulent zones.

Some additional observations can be made.

(i) The dissipation is higher in the central region of the jet than near its boundaries. The conventionally averaged dissipation decreases monotonically

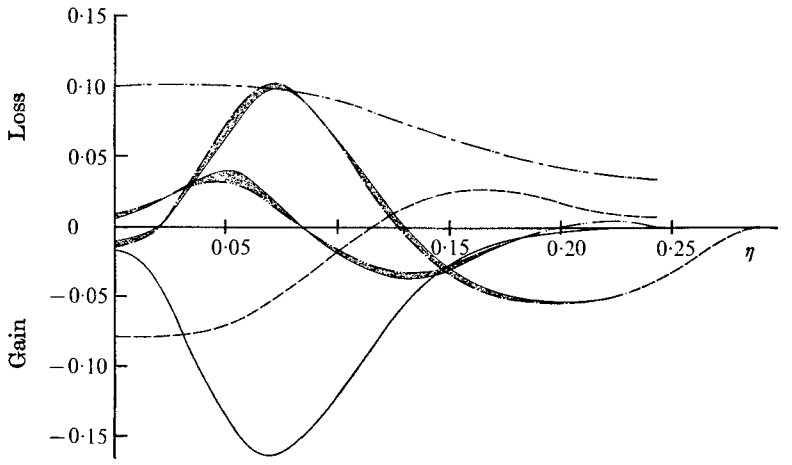

FIGURE 29. The turbulent energy balance. ——, production; — —, convection; —···—, diffusion; —·-·—, dissipation; —·—, pressure transport.

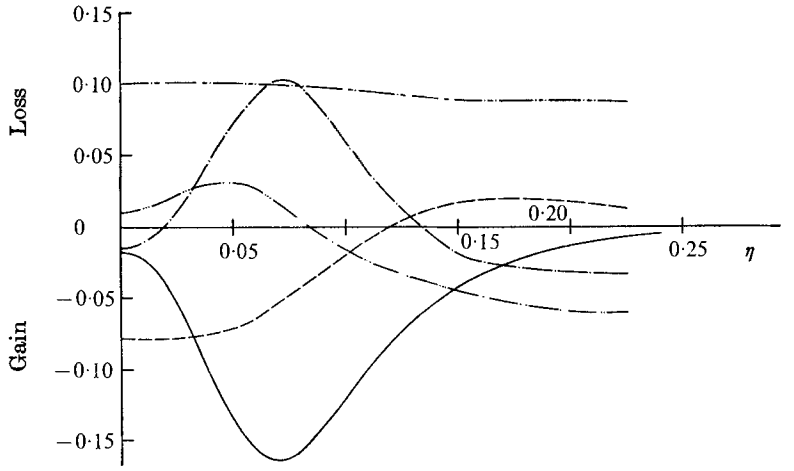

FIGURE 30. The turbulent energy balance in the turbulent zone. Curves as in figure 29.

with η for $\eta > 0{\cdot}05$ while the dissipation in the turbulent zone is almost constant across the jet.

(ii) The production is highest at an η corresponding approximately to the location of the highest shear stress. The maximum level of the production term is almost double the maximum level of the dissipation term. The production in the turbulent zone is very nearly the same as the conventionally averaged result.

(iii) Most of the turbulent energy gained at the centre is by convection. For $\eta \leqslant 0{\cdot}05$ the convection term is comparable to the dissipation.

(iv) In the outer part of the jet ($\eta \geqslant 0{\cdot}2$) the diffusion term is equal to the sum of all the other terms in the energy budget. The conventionally measured diffusion term has a minimum at $\eta = 0{\cdot}2$ and probably returns to zero at larger η. The diffusion in the turbulent zone remains constant at large η.

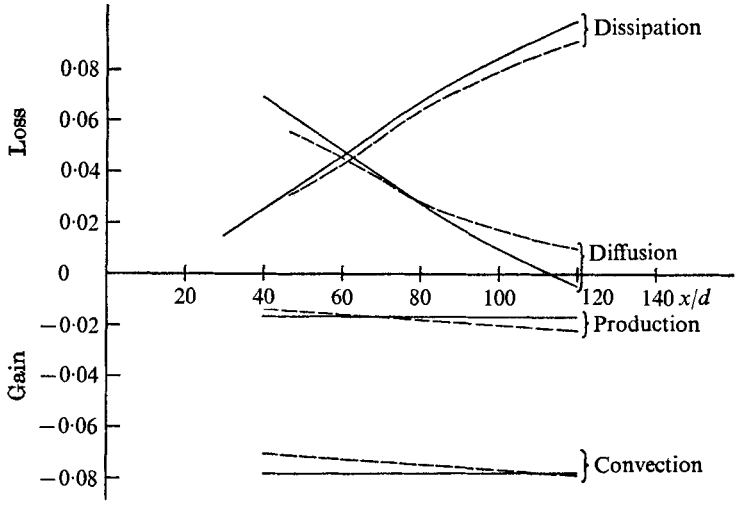

FIGURE 31. Axial distribution of the energy balance on the centre-plane. ——, Heskestad (1965); ——, present measurements.

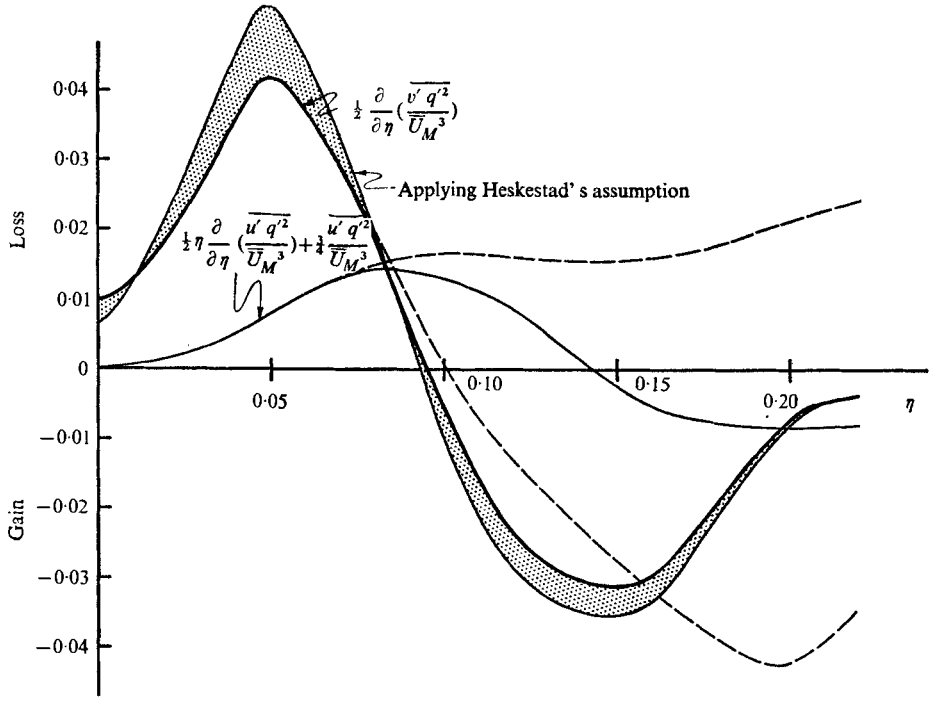

FIGURE 32. The distribution of the axial and lateral diffusion across the jet. ——, conventional; — —, turbulent zone.

(v) A breakdown of the diffusion term is shown in figure 32. The lateral velocity fluctuations transport turbulent energy from the central region of the jet to its outskirts, i.e. from a region where the intensity is high to a region where it is relatively low. The effect of the assumed $\overline{v'w'^2}/\overline{U}_M^3$ on the lateral diffusion term is not large in spite of the fact that $(\overline{v'w'^2}/\overline{U}_M^3)_{\max}$ is 2·5 times larger than the measured quantity. The effect the assumed quantity has on the pressure transport is shown in figure 29. The discrepancy between the two pressure-transport curves may be considered as experimental uncertainty. Since there is also a gradient of turbulent energy in the axial direction, energy is transported downstream (i.e. lost) by the axial fluctuations.

(vi) The energy transported from the centre of the jet outwards is partly lost by dissipation and partly by axial diffusion. The mechanism is very clearly visible in the turbulent zone-averaged energy balance (figures 30 and 32). The weighting of the data by intermittency masks this effect in the conventional budget of turbulent energy.

The production and convection terms on the axis of the jet (figure 31) are independent of the distance from the nozzle. The dissipation term increases linearly with x and hence the pressure-transport term decreases accordingly. The results are in fairly good agreement with those computed by us from Heskestad's raw data.

The kinetic energy of the mean motion across the jet was computed from the equation

$$0 = \frac{1}{2}\frac{d}{dx}\int_0^\infty \overline{U}^3 dy + \int_0^\infty \overline{U}\frac{\overline{\partial u'v'}}{\partial y}dy - \nu\int_0^\infty \overline{U}\frac{\partial^2\overline{U}}{\partial y^2}dy + \int_0^\infty \overline{U}\frac{\partial}{\partial x}(\overline{u'^2}-\overline{v'^2})\,dy,$$

which reduces in the self-preserving region to

$$\frac{1}{4}\int_0^\infty \left(\frac{\overline{U}}{\overline{U}_M}\right)^2 d\eta = \int_0^\infty \frac{\overline{u'v'}}{\overline{U}_M^2}\frac{\partial(\overline{U}/\overline{U}_M)}{\partial\eta}d\eta - \frac{\nu}{\overline{U}_M x}\int_0^\infty \frac{\overline{U}}{\overline{U}_M}\frac{\partial^2(\overline{U}/\overline{U}_M)}{\partial\eta^2}d\eta - \int_0^\infty \frac{\overline{U}}{\overline{U}_M}\left(\frac{\overline{u'^2}-\overline{v'^2}}{\overline{U}_M^2}\right)d\eta.$$

This equation represents the rate of transformation of mean kinetic energy into turbulent energy (i.e. turbulent production) and the dissipation by viscous forces.

From the conventional measurements we find the various integrals to be equal:

$$\tfrac{1}{4}\times 0{\cdot}061 = -0{\cdot}0167 + (\nu/\overline{U}_M x)\,5{\cdot}196 - 0{\cdot}0048,$$

i.e. the kinetic energy at any cross-section of the jet is given by

$$E = 0{\cdot}0367 - 2{\cdot}2\,Re^{-1}(x/d)^{-\frac{1}{2}},$$

where $Re = U_0 d/\nu$ is the Reynolds number at the nozzle. Thus the mass flow in the jet increases with $x(Q = 0{\cdot}122\,(x/d)^{\frac{1}{2}})$, the momentum remains constant and the energy drops as $x^{-\frac{1}{2}}$.

The mass flux in the turbulent zone can not be computed very accurately because the velocity does not vanish at large η. Nevertheless Q_T was computed and found to be approximately equal to $0{\cdot}144(x/d)^{\frac{1}{2}}$. $Q_T > Q$ because we assumed

that the entire jet is filled with turbulent fluid; this of course never happens over an extended period of time. Similarly the energy flux is given by

$$E_T = 0{\cdot}0381 - 2{\cdot}02\,Re^{-1}(x/d)^{-\frac{1}{2}}.$$

E_T is again larger than E because we have excluded the contortions of the interface from these calculations.

9. Some concluding remarks

The two-dimensional jet becomes self-preserving about 40 slot widths downstream from the nozzle. There is some scant evidence that self-preservation may not be universal but depends to a degree on the initial conditions. There are differences of approximately 10 % in the spread of the jet, differences in the decay of its maximum velocity and differences in the location of its hypothetical origin as well as differences in the lateral distribution of all three components of the turbulent intensity which can easily be attributed to the different initial conditions. A carefully controlled experiment linking the initial conditions to the far-field flow certainly seems worth while at this stage.

Three free shear flows, the axisymmetric jet, the two-dimensional jet and the mixing layer, have now been investigated using essentially identical equipment and procedures. Hence, whatever errors were made in one were most probably made in the others.

The axisymmetric jet is similar to the two-dimensional jet in its distribution of mean velocity, intermittency, turbulent intensities, etc. All three flows indicate a definite lack of isotropy even in the high wavenumber range, however the two-dimensional jet seems to be the most appropriate configuration for further study in the laboratory of the question of local isotropy.

The differences between the turbulent zone-averaged results and the conventional results in the two-dimensional jet are not large except for $\overline{u'v'}$ and third-order correlations. It is suggested that the very strong diffusion at the outer edge of the turbulent zone in both the mixing layer and the jet should be investigated.

This paper is based on the master's thesis of the first author. It was initiated in 1969 by the second author, who spent a sabbatical year at the Technion. The measurements were completed in 1973. During the final stages of the investigation the work was supported in part by Grant AFOSR-72-2346 from the Air-Force Office of Scientific Research, made to the second author at Tel-Aviv University.

REFERENCES

BATT, R. G., KUBOTA, T. & LAUFER, J. 1970 *A.I.A.A. Paper*, no. 70–721.

BRADBURY, L. J. S. 1965 *J. Fluid Mech.* **23**, 31.

CHAMPAGNE, F. H., PAO, Y. H. & WYGNANSKI, I. J. 1973 *University of California, San Diego, A.M.E.S. Dept. Rep.* AFOSR 72–2287.

CROW, S. C. & CHAMPAGNE, F. H. 1971 *J. Fluid Mech.* **48**, 547.

FÖRTHMANN, E. 1934 *Ing. Arch.* **5**, 42.

GRANT, H. L., STEWART, R. W. & MOILLIET, A. 1962 *J. Fluid Mech.* **12**, 241.

HESKESTAD, G. 1965 *J. Appl. Mech.* **32**, 721.

JEROME, F. E., GUITTON, D. E. & PATEL, R. P. 1971 *Aero. Quart.* **23**, 119.

KNYSTAUTAS, R. 1964 *Aero. Quart.* **15**, 1.

MILLER, D. R. & COMINGS, E. W. 1957 *J. Fluid Mech.* **3**, 1.

TOWNSEND, A. A. 1949 *Proc. Roy. Soc.* A **197**, 124.

TOWNSEND, A. A. 1956 *The Structure of Turbulent Shear Flow.* Cambridge University Press.

VAN DER HEGGE ZIJNEN, B. G. 1958 *Appl. Sci. Res.* A **7**, 293.

WYGNANSKI, I. 1964 *Aero. Quart.* **15**, 373.

WYGNANSKI, I. & FIEDLER, H. E. 1969 *J. Fluid Mech.* **38**, 577.

WYGNANSKI, I. & FIEDLER, H. E. 1970 *J. Fluid Mech.* **41**, 327.

WYNGAARD, J. C. 1969 *J. Sci. Instrum. Ser.* 2, **2**, 983.